

Modelling and experimental validation of a fluidized-bed reactor freeboard region: Application to natural gas combustion

S. Dounit, M. Hemati*, R. Andreux

Laboratoire de Génie Chimique, U.M.R. 5503, ENSIACET, 05 rue Paulin Talabot, 31106 Toulouse, France

Received 17 September 2007; received in revised form 14 November 2007; accepted 16 November 2007

Abstract

A theoretical and experimental study of natural gas–air mixture combustion in a fluidized bed of sand particles is presented. The operating temperatures are lower than a critical temperature of 800 °C above which the combustion occurs in the vicinity of the fluidized bed. Our study focusses on the freeboard zone where most of the methane combustion takes place at such temperatures. Experimental results show the essential role of the projection zone in determining the global thermal efficiency of the reactor. The dense bed temperature, the fluidizing velocity and the mean particle diameter significantly affect the thermal behaviours.

A model for natural gas–air mixture combustion in fluidized beds is proposed, counting for interactions between dense and dilute regions of the reactor [P. Pré, M. Hemati, B. Marchand, Study of natural gas combustion in fluidised beds: modelling and experimental validation, *Chem. Eng. Sci.* 53 (1998) (16), 2871] supplemented with the freeboard region modelling of Kunii–Levenspiel [D. Kunii, O. Levenspiel, Fluidized reactor models: 1. For bubbling beds of fines, intermediate and large particles. 2. For the lean phase: freeboard and fast fluidization, *Ind. Eng. Chem. Res.* 29 (1990) 1226–1234]. Thermal exchanges due to the convection between gas and particles, and due to the conduction and radiation phenomena between the gas-particle suspension and the reactor walls are counted. The kinetic scheme for the methane conversion is that proposed by Dryer and Glassman [F.L. Dryer, I. Glassman, High-temperature oxidation of CO and CH₄, Proceedings of the 14th International Symposium on Combustion, The Combustion Institute, Pittsburg (1973) 987]. Model predictions are in good agreement with the measurements.

© 2007 Elsevier B.V. All rights reserved.

Keywords: Fluidization; Combustion; Natural gas; Model; Freeboard

1. Introduction

Fluidized-bed combustors have many advantages, including their simplicity of construction, their flexibility in accepting solid, liquid or gaseous fuel, and their high-combustion efficiency at low temperatures what minimises *NO_x* generation [1]. Fluidized-bed natural gas combustors are used in many industrial applications such as incineration of sludge with high-moisture content or solid particles calcination. Given the ecological benefit of using natural gas in fluidized-bed furnaces, it is of interest to describe the combustion process in fluidized beds using experimental and theoretical approaches.

Natural gas combustion mechanisms in fluidized beds have been widely investigated at bed temperatures greater than a critical temperature close to 800 °C [2–7], above which the methane

conversion is fully realized in the dense zone. Sadirov and Baskakov [8] reported temperatures measured in the bubble-eruption zone above the bed surface greater than the theoretical flame temperature. At bed temperatures lower than this critical temperature, the combustion of methane is mainly realized in the freeboard zone. In such conditions, the methane bubble eruption in the lean phase of the fluidized-bed induces high-exploding risks [2]. Thus, low temperature reacting fluidized-bed applications require experiments for safety reasons. In such a way, hydrodynamics and thermal phenomena occurring in the freeboard region of fluidized-bed reactors must be investigated and modelled.

However, there is a lack of references in the literature on the experimental and theoretical study of the reacting fluidized-bed dilute region. Indeed, previous works were either room temperature hydrodynamic studies [9–13] or isothermal catalytic chemical studies.

In this paper, hydrodynamics and thermal phenomena coupling in the projection zone of a fluidized-bed operating in the

* Corresponding author.

E-mail address: regis.andreux@ensiacet.fr (M. Hemati).

Nomenclature

A	reactor cross-sectional area (m^2).
C_i	concentration of species i in gas stream (mol m^{-3}).
C_{ps}	specific heat of particles ($\text{J kg}^{-1} \text{K}^{-1}$).
D_r	reactor diameter (m).
d_p	mean particle diameter (m).
dh_i	height of compartments i (m).
E_i	heat flux emitted by radiation from slice i and originate from this slice in one direction. The total heat flux emitted being $2E_i$ (W).
f_v	volume fraction of particles in each freeboard compartment.
f_w	bubbles volume fraction occupied by the wake.
F	flux of entrained particles ($\text{kg m}^{-2} \text{s}^{-1}$).
F_0	flux of entrained particles at dense bed surface ($\text{kg m}^{-2} \text{s}^{-1}$).
h	height above the bed surface (m).
h_{gp}	heat transfer coefficient by convection between gas and solid particles ($\text{W m}^{-2} \text{K}^{-1}$).
h_{pw}	heat transfer coefficient by conduction and radiation between the gas-particle suspension and reactor-walls ($\text{W m}^{-2} \text{K}^{-1}$).
H_i	molar enthalpy of species i (J mol^{-1}).
k_g	gas phase conductivity ($\text{W m}^{-1} \text{K}^{-1}$).
L	characteristic height of a freeboard compartment (m).
L_g	gas film thickness (m).
ΔP_i	mean pressure drop (Pa).
q_c	heat flux exchanged by conduction between the gas–solid suspension and reactor walls (W m^{-2}).
q_{re}	heat flux exchanged by radiation between the gas–solid suspension and reactor walls (W m^{-2}).
$q_{tot i}$	heat flux absorbed by slice i and coming from all other regions per unit surface (W m^{-2}).
r_i	reaction rate for every gas species i ($\text{mol m}^{-3} \text{s}^{-1}$).
R	reactor radius (m).
T_g	gas temperature (K).
T_p	particle temperature (K).
T_w	reactor wall temperature (K).
T_{bed}	dense bed average temperature (K).
U_g	superficial gas velocity (m s^{-1}).
U_i	interstitial gas velocity (m s^{-1}).
U_{mf}	minimum fluidizing velocity of solid particles (m s^{-1}).
y_i	mole fraction of species i in gas stream.
Z	height above the gas distributor (m).

Greek letters

ε	local freeboard voidage.
$\bar{\varepsilon}_g$	gas-particles suspension emissivity.
ε_p	particles emissivity
ε_w	emissivity of reactor walls.

ε_{mf}	dense bed voidage at minimum fluidizing conditions.
η	contact efficiency at height h .
η_{bed}	contact efficiency at bed surface.
ρ	gas-particle suspension density (kg/m^3).
ρ_s	density of the particles (kg/m^3).
ρ_0	gas-particle suspension density at bed surface (kg/m^3).
σ	Stefan–Boltzmann constant ($5.67 \cdot 10^{-8} \text{ W/(m}^2 \text{ K}^4)$).
σ_i	standard deviation of pressure drop fluctuations (Pa).

Dimensionless numbers

Reynolds number $Re = (\rho_g U_i d_p) / \mu_g$

Prandtl number $Pr = (\mu_g C_{pg}) / k_g$

bubbling regime is experimentally studied and modelled. The natural gas combustion modelling proposed by Pré et al. [3] is used to predict the reactor dense region while the Kunii and Levenspiel modelling [12] is used to describe the freeboard region. The two-stage kinetic scheme of methane conversion proposed by Dryer and Glassman [14] is used. The resulting reactor model is validated using our experimental data.

2. Description of the setup

The experimental setup is given in Fig. 1. The reactor consists of a heat resistant of steel pipe 180 mm in diameter and 1400 mm high, with a disengaging section 360 mm in diameter and 1000 mm high. The reactor is equipped with a perforated plate distributor of 1.8% porosity. The bed temperature is controlled using cooling air flowing in a double shell. The pneumatic valve what controls the air circuit feeding into the double shell is controlled by a PID system equipped with a thermocouple located in the dense bed. Natural gas with 97% methane content is used as the combustible and premixed to the air in the windbox. The reactor is fitted axially with chromel–alumel-type temperature sensors and water-cooled tubes to sample the gas located at 50, 100, 250, 300, 400, 450, 550, 600, 650, 700, 900, 1000, 1100, 1200 and 1300 mm above the distributor. The sampling tubes are connected to a pump, a cooling unit to eliminate water, infrared-type analysers to measure CH_4 , CO_2 , and CO mole fractions, and a paramagnetic-type analyser for O_2 measurements. Experiments safety is ensured using (i) a burner placed in the wider section of the reactor what converts the unburned gas exiting at the fluidized-bed outlet and (ii) a thermocouple placed in the windbox connected to a PID regulator what cuts off the reactor feeding when the windbox temperature reaches a critical value chosen well below the air–methane auto-burning temperature.

The studied operating conditions are presented in Table 1. Typical sand particles with a density of 2650 kg m^{-3} and mean size ranging between 100 and $550 \mu\text{m}$ are fluidized. The air factor, defined as the ratio of the volume of air fed into the

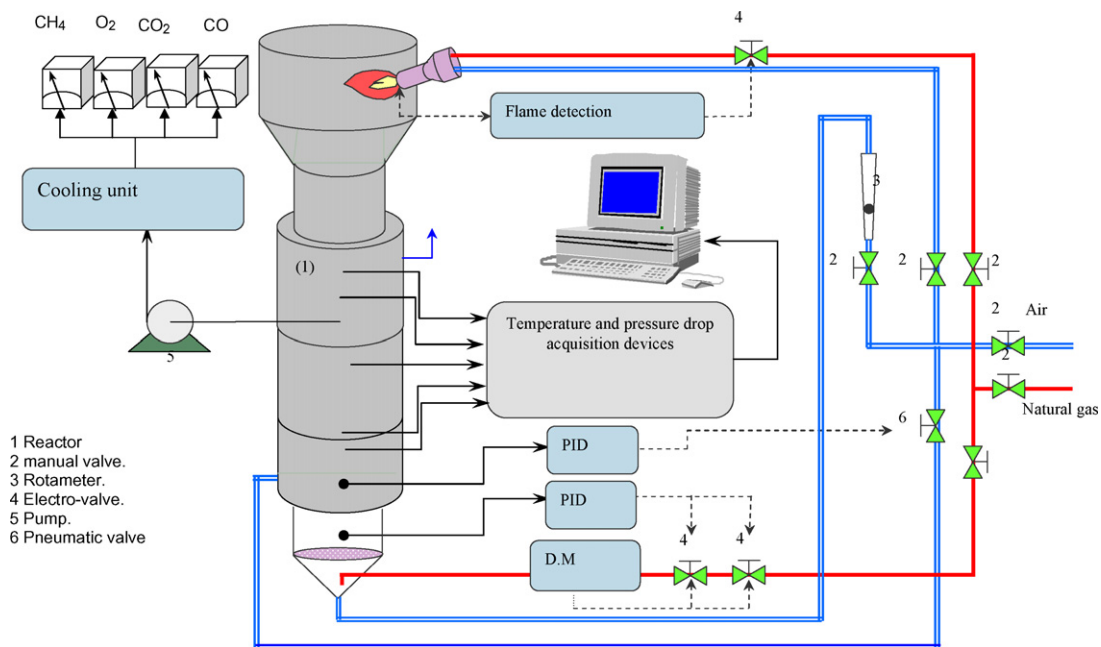


Fig. 1. Schematic of the setup.

reactor to the required volume for stoichiometric combustion of methane, ranges between 1.0 and 1.5. The bed temperature, T_{bed} , is defined to that measured 150 mm above the distributor. The fluidizing velocity ranges between two and four times the minimum fluidizing velocity at 20 °C.

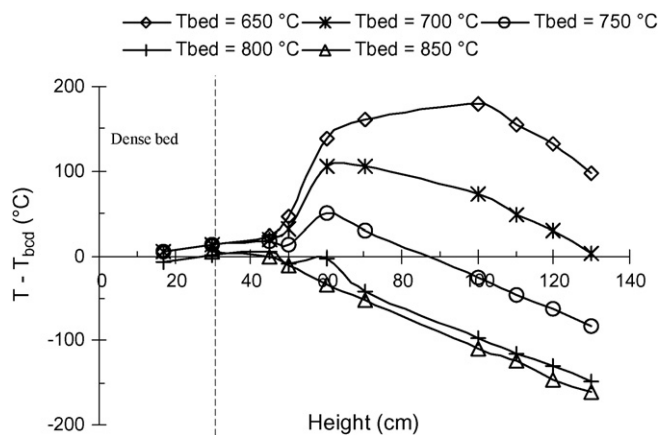
3. Experimental results

3.1. Typical experiment presentation

C1 experiments (Table 1) are realized in permanent regime, with a dense bed temperature ranging between 650 and 800 °C.

3.1.1. Temperature profiles

The differences between the local temperature measured along the reactor axis and the dense bed temperature, T_{bed} , are presented in Fig. 2. An increase in the local temperature characterizes the combustion zone, what moves towards the bed surface when increasing the dense bed temperature. The combustion mainly takes place in the bed dense region when dense bed tem-

Fig. 2. Evolution of the difference $T - T_{bed}$ along the reactor for different dense bed temperatures.

perature is higher than 800 °C, what is consistent with previous observations reported in the literature [15,3,4]. The local temperature decreasing above the combustion zone is attributed to heat losses.

Table 1
Operating conditions of premixed air-natural gas combustion experiments

Experience	Solid mass (kg)	U_g/U_{mf} at 20 °C	Excess air factor	d_p (μm)	Variable parameter
C1	12	2	1.2	350	Reference
C2	9	2	1.2	350	Solid mass
C3	15				
C4	12	3	1.2	350	Superficial gas velocity
C5		4			
C6	12	2	1	350	Excess air factor
C7			1.5		
C8	12	2	1.2	100	Mean particle diameter
C9				550	

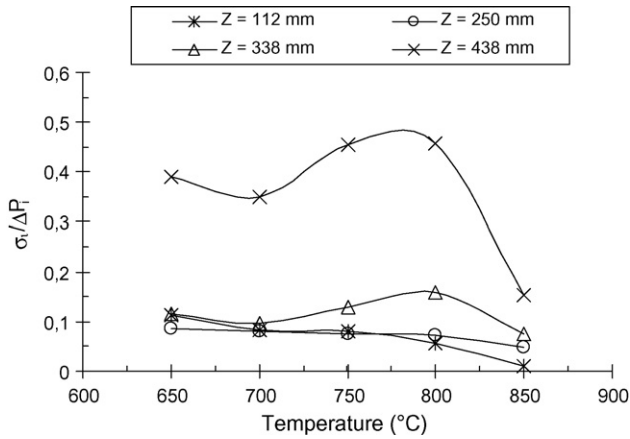


Fig. 3. Normalised standard deviation of pressure drop fluctuations at different heights in the reactor against dense bed temperature.

3.1.2. Pressure drop profiles

The effect of the dense bed temperature, T_{bed} , on the normalized standard deviation of the pressure drop fluctuations, $\sigma/\Delta P$, measured at different heights is presented in Fig. 3. The methane combustion occurs close to the bed surface when the dense bed temperature, T_{bed} , reaches the critical value of 800 °C, and the resulting exploding of methane bubbles reaching the bed surface induces an increase in the local pressure fluctuations. When increasing the bed temperature above the critical temperature, T_{bed} , the local pressure fluctuations decrease again. Such observations have ever been reported by Baskakov and Makhorin [7].

3.1.3. Reaction behaviour

The freeboard region plays an important role in the combustion behaviour, especially when the dense bed temperature is lower than the critical value of 800 °C. At a dense bed temperature, T_{bed} , of 700 °C, the major part of the methane conversion is realized in the freeboard region 400 mm above the dense bed surface, as underlined by the mole fraction of the stable species (CH_4 , O_2 , CO_2) measured along the reactor axis (Fig. 4a). The progressive decreasing in the local methane mole fraction indicates that the natural gas combustion process in the freeboard region of the reactor is a progressive process.

The bell shape of the CO mole fraction profile confirms the successive nature of the methane combustion reaction with CO formation as an intermediate species (Fig. 4b). This was already observed experimentally and modelled by several authors [14,16,17].

3.2. Effect of operating conditions

The experiments are carried out at dense bed temperatures lower than the critical temperature of 800 °C (Table 1). An increase in the excess air factor above 1.1 has little influence on the process behaviour, both in the dense and dilute regions. The temperature and the methane conversion profiles obtained at different excess air factors are very close to each other [15]. On the other hand, an increase in the total mass of solids in the reactor from 9 up to 15 kg has no significant effect on the reac-

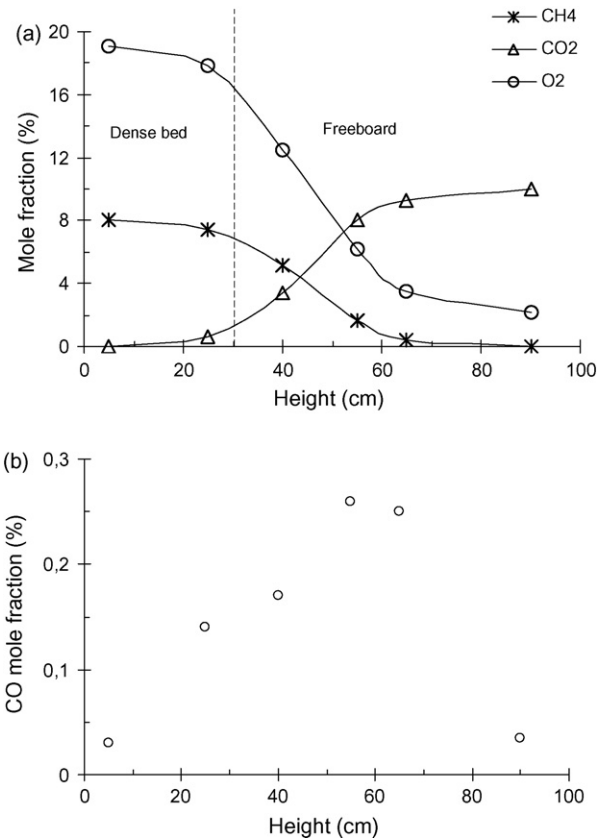


Fig. 4. (a) Mole fraction profiles of stable chemical species (Test C1, $T_{\text{bed}} = 700$ °C). (b): CO mole fraction profile (Test C1, $T_{\text{bed}} = 700$ °C).

tion progress in the freeboard, since no reaction occurs in the dense bed region at these low bed temperatures.

3.2.1. Superficial gas velocity effect

Figs. 5 and 6 present the temperature and the methane conversion measured along the reactor axis at 700 °C. Three values of gas velocity are considered, respectively 2, 3 and 4 times U_{mf} at 20 °C, corresponding to gas velocities ranging between 10.5 and 26 times U_{mf} at dense bed temperature. The combustion zone moves upwards from the bed level to the outlet of the reactor when increasing the superficial gas velocity. This occurs

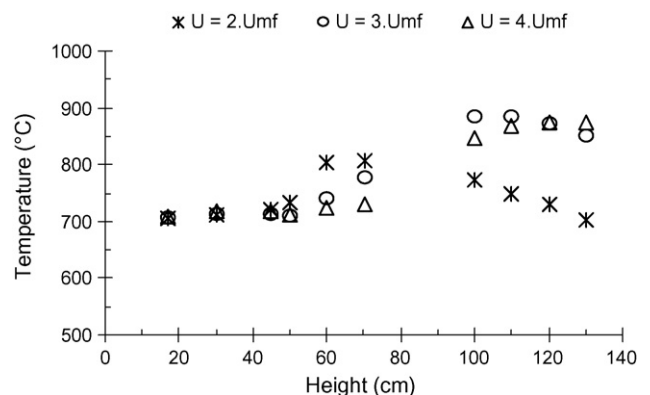


Fig. 5. Temperature profiles obtained at $T_{\text{bed}} = 700$ °C for three values of gas velocity.

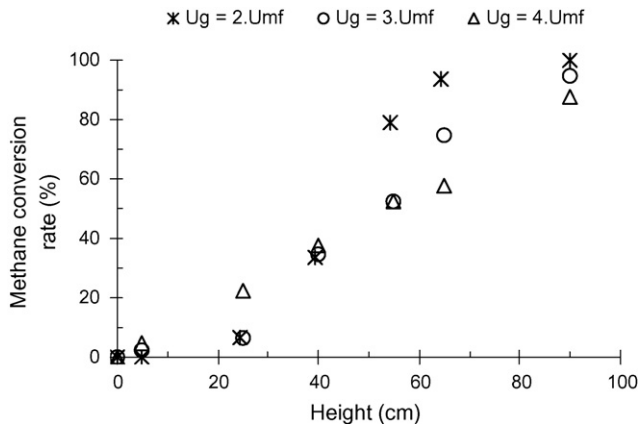


Fig. 6. Methane conversion rate profiles at $T_{\text{bed}} = 700^\circ\text{C}$ for three values of gas velocity.

because an increase in the gas velocity leads to a decrease in the mean residence time of reactants in the reactor, and also to an enhancement of the projection height of solid particles. These projected particles contributes to the dilute phase temperature increasing and thus on the combustion. Results obtained at bed temperatures lower than 750°C were similar to those presented in this section for 700°C .

3.2.2. Mean particle diameter effect

The effect of the mean particle diameter has been investigated between 100 and $550\ \mu\text{m}$ (runs C1, C8 and C9 in Table 1). The superficial gas velocity was kept constant; equivalent to twice the minimum fluidization velocity of particles $350\ \mu\text{m}$ in diameter at 20°C . Fig. 7 presents the methane conversion as a function of the height at 700°C for each size of particles. Decreasing the mean particle diameter makes the combustion zone move upwards to the reactor outlet, what is a consequence of the significant enhancement of two parameters: the direct contact surface between gas and solid particles, and the particles hold-up in the freeboard region, caused by an increase in the bubbles velocity and diameter at the dense bed surface. At constant fluidizing velocity, decreasing the particle size leads to an increase in the excess gas velocity ($U_g - U_{\text{mf}}$) what affects strongly the bubble size and velocity. Similar behaviour was observed at the other dense bed temperatures tested in this work.

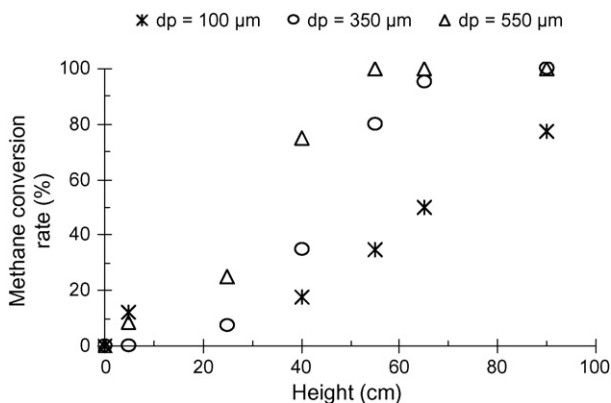


Fig. 7. Methane conversion rate at 700°C for three particle sizes.

4. Reactor model

The model for natural gas combustion process in the dense zone of the reactor is based on the bubble assemblage model introduced by Kato and Wen [18] what has been improved to count for the thermal transfer that occurs during the combustion. It has ever been validated at dense bed temperatures greater than 850°C [3]. The model is supplemented with a freeboard modelling to count for the strong effects we experimentally evidenced of the freeboard on the global bed combustion when the bed temperature T_{bed} is kept lower than the critical temperature of 800°C . The following assumptions are considered:

- (I) The freeboard region is fed only by the gas contained in bubbles; the temperature and composition of which are that of the bubble phase at the bed surface.
- (II) The projected particles originate from the bubble wakes. They are projected by packets having initial velocities equal to the bubble rise velocity at the dense bed surface.
- (III) The particle projection by packets makes only a fraction of their total surface accessible to gas. A contact efficiency factor is thus introduced.
- (IV) The entrained particle flux, the contact efficiency factor and the solid hold-up along the freeboard fall exponentially from their values at the dense bed surface.
- (V) The gas phase and the particle phase flows are plug flows without and with back flow, respectively.
- (VI) The freeboard region is subdivided into a number of elementary compartments.

4.1. Heat transfer in the freeboard

The following mechanisms are counted in the modelling:

- (1) the gas-to-particle convection.
- (2) the gas-particle-suspension-to-reactor-wall conduction and radiation.
- (3) the particle-to-particle radiation.

As a first approximation, the radial heat transfer resistance is assumed to be located in a thin film at the reactor wall.

The convective heat transfer coefficient between gas and solid particles is modelled using the Ranz and Marshall's [22] correlation.

4.1.1. Gas-particle suspension to reactor-wall transfer

The model is similar to that proposed by Kunii and Levenspiel [19] for the dense region of the reactor. The heat flow exchanged between the gas-particle suspension and the reactor wall is the sum of conductive and radiative contributions:

$$q = q_c + q_{\text{re}} \quad (1)$$

Since the extinction coefficient ($\tau_p = 1.5 f_v \varepsilon_p / d_p$) is much higher than unity (3.85 for a system with 1% solid hold-up and $350\ \mu\text{m}$ mean particle diameter), the gas–solid suspension is considered as a grey surface as well as the reactor-wall. Thus,

the radiative contribution can be written

$$q_{re} = \frac{\sigma(T_p^4 - T_w^4)}{(1/\varepsilon_w) + (1/\bar{\varepsilon}_g) - 1} \quad (2)$$

where ε_g is the gas-particles suspension emissivity, what depends both on the emissivity of the gas phase and the local particles concentration. Its value is estimated using the correlation reported in Appendix A.

The conductive contribution is governed by the conduction through a gas film near the reactor wall. Its thickness can be estimated as $L_g = d_p/2$. This contribution is expressed, according to Kunii and Levenspiel, as

$$q_c = \frac{k_g}{L_g} \cdot (T_p - T_w) \quad (3)$$

4.1.2. Axial radiative heat transfer between different regions of the freeboard

Various experimental measurements have shown that when the natural gas combustion occurs partially or totally in the freeboard zone, the temperature and the solid hold-up varies continuously along the reactor axis [2,15]. These gradients generate an axial radiative heat transfer which can significantly affect the chemical reaction.

An approach similar to that proposed by Bueters et al. [20] was used in this work. The freeboard zone is discretized into N compartments separated by virtual planes. The radiative heat flux absorbed by each slice i of the freeboard and coming from all other freeboard slices can be expressed as

$$q_{tot i} = \bar{\varepsilon}_{gi} \cdot (E_{i-1} + E_{i+1}) + \sum_{j=1}^{j=i-2} \left(E_j \bar{\varepsilon}_{gi} \prod_{k=i-1}^{j+1} (1 - \bar{\varepsilon}_{gk}) \right) + \sum_{j=i+2}^N \left(E_j \cdot \bar{\varepsilon}_{gi} \cdot \prod_{k=i+1}^{j-1} (1 - \bar{\varepsilon}_{gk}) \right) \quad (4)$$

where E_j represents the radiative heat flow emitted in one direction by slice j

$$E_j = \frac{1}{2} \bar{\varepsilon}_{gj} \sigma (2A) T_j^4 \quad (5)$$

4.2. Hydrodynamics of the system

Modelling of natural gas combustion in the freeboard region of a fluidized-bed reactor necessitates prior knowledge of the solid hold-up and the flux of projected particles along this region. In Table 2, we present the correlations used.

Table 2
Correlations used for the hydrodynamic parameters

Variable	Correlation	Reference
Solid hold-up	$\rho = \rho_0 \exp(-ah)$	[12]
Entrainment	$F = F_0 \exp(-ah)$	[19]
Flux of particles projected at the bed surface	$F_0 = \frac{1}{2} f_w (1 - \varepsilon_{mf}) \rho_s (U_g - U_{mf})$ with $f_w = 0.25$	[19]
Contact efficiency factor	$1 - \eta = (1 - \eta)_{bed} \exp(-a'h)$ with $a' = 6.62 \text{ m}^{-1}$	[19]
Exponential factor "a"	Graphical correlation of Kunii and Levenspiel [12]	[12]

4.3. Model equations

The mass balance is written for every principal species present in the gas phase (CH_4 , O_2 , N_2 , H_2O , CO , CO_2 , and NO) while the heat balances are established separately both for gaseous and particulate phases (Table 3).

The model equations are solved in three steps:

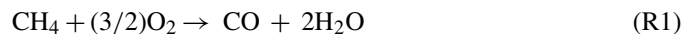
- (I) Initially the heat and mass balances for each compartment of the dense region are solved.
- (II) Secondly, for each slice of the freeboard zone, the heat and mass balances are solved.
- (III) Finally the global heat and mass balances for the entire reactor is checked.

The systems of equations obtained both for the dense and for the freeboard zones are non-linear algebraic systems solved using the Newton–Raphson method. More details can be found in Pré-Goubelle [4] and Dounit [15]. From this procedure, we get the axial profiles of different species mole fractions present in the gas stream and both gas and particle temperatures profiles along the reactor. The heat loss due to conduction and radiation to external medium can also be computed.

5. Discussion of the model results

5.1. Kinetic scheme

The kinetic schemes available of Dryer and Glassman [14], Westbrook and Dryer [16], and Bradley et al. [17] have been tested and compared to our experiments. The one of Dryer and Glassman [14] gives the best predictions. Only the results obtained with this kinetics scheme are discussed here



The rates of reactions R1 and R2 and the values of kinetic parameters involved are reported in Table 4.

At relatively low temperatures (less than 750°C), good agreement has been obtained for kinetic parameters giving the fastest reaction rate for methane transformation ($n = 13.4$ and $E = 197.768 \text{ kJ mol}^{-1}$), as shown in Figs. 8 and 9. At dense bed temperatures closer to the critical temperature of 800°C , the best agreement was obtained for kinetic parameters of methane transformation reaction closer to the mean values proposed by Dryer and Glassman ($n = 13$ and $E = 197.768 \text{ kJ mol}^{-1}$) as seen

Table 3

Model equations (heat and mass balances)

Mass balance

$$3[U_g C_i]^N - 4[U_g C_i]^{N-1} + [U_g C_i]^{N-2} - 2\varepsilon_N r_i dh_N = 0, \quad i = 1, Nc$$

Heat balance

Gas phase

$$3 \left[\frac{U_g}{T_g} \sum_{i=1}^{NC} y_i H_i \right]^N - 4 \left[\frac{U_g}{T_g} \sum_{i=1}^{NC} y_i H_i \right]^{N-1} + \left[\frac{U_g}{T_g} \sum_{i=1}^{NC} y_i H_i \right]^{N-2} + 2 \frac{6}{d_p} (1 - \varepsilon_N) h_{gp} \frac{R}{P} (T_g|^N - T_p|^N) \bar{\eta}_N dh_N = 0$$

Particulate phase

$$\left\{ F_a |^{N-1} C_{ps} A(T_p |^{N-1} - T_{ref}) + F_d |^{N-1} C_{ps} A(T_p |^{N-1} - T_{ref}) + \frac{6}{d_p} (1 - \varepsilon_N) \bar{\eta}_N h_{gp} A(T_g |^N - T_p |^N) dh_N + q_{tot N} \right\} - \quad i$$

$$\{ [F_a + F_d]^N C_{ps} A(T_p |^N - T_{ref}) + 2\sigma A \bar{\varepsilon}_{gN} (T_p |^N)^4 + h_{pw} (\pi D_r dh_N) (T_p |^N - T_w \text{ int}) \} = 0 \quad \begin{array}{l} 1 \\ 2 \\ 3 \\ 4 \\ 5 \\ 6 \\ 7 \end{array} \quad \begin{array}{l} \text{CH}_4 \\ \text{O}_2 \\ \text{N}_2 \\ \text{CO}_2 \\ \text{H}_2\text{O} \\ \text{CO} \\ \text{NO} \end{array}$$

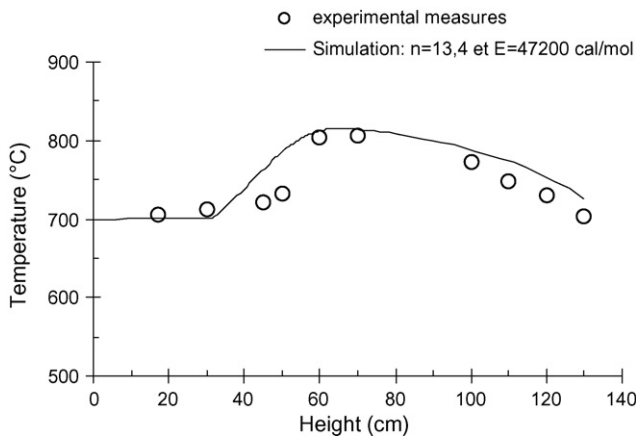
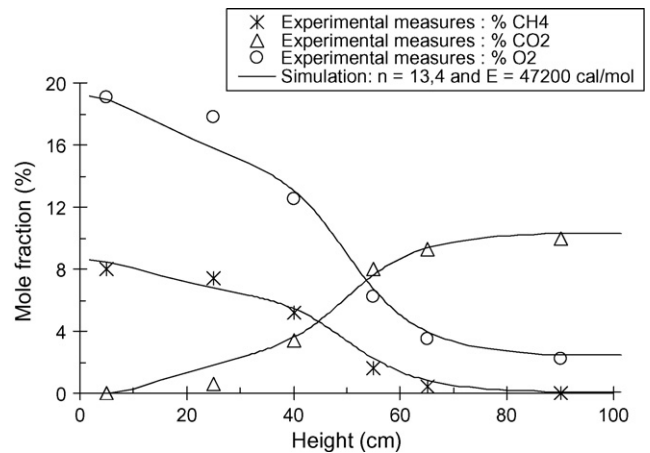
$$\text{Particles to reactor wall heat transfer coefficient: } h_{pw} = \frac{k_g}{L_g} + \frac{\sigma(T_p + T_w)(T_p^2 + T_w^2)}{(1/\varepsilon_w) + (1/\varepsilon_g) - 1}$$

$$\text{Gas-to-particle heat transfer coefficient: } h_{gp} = \left(\frac{k_g}{d_p} \right) \cdot (2 + 0.6Re^{1/2} Pr^{1/3})$$

Table 4

Reaction rate expressions and kinetic parameters values according to Dryer and Glassman [14]

Reaction	Reaction rate expression	Kinetic parameters
R1	$r_{\text{CH}_4} = -10^n C_{\text{CH}_4}^{0.7} C_{\text{O}_2}^{0.8} \exp \left[-\frac{E \times 4.18}{RT} \right] \times 10^{-3}$	$n = 13.2 \pm 0.2$ $E = 48,400 \pm 1200 \text{ (cal mol}^{-1}\text{)}$
R2	$r_{\text{CO}} = -10^n C_{\text{CO}} C_{\text{O}_2}^{0.25} C_{\text{H}_2\text{O}}^{0.5} \exp \left[-\frac{E \times 4.18}{RT} \right] \times 10^{-4.5}$	$n = 14.75 \pm 0.4$ $E = 43,000 \pm 2200 \text{ (cal mol}^{-1}\text{)}$

Fig. 8. Temperature profile of gas-particles suspension: comparison between the experimental results and the model predictions ($T_{\text{bed}} = 700^\circ\text{C}$).Fig. 9. Mole fraction profiles of the main species present in gas stream: comparison between the experimental results and the model predictions ($T_{\text{bed}} = 700^\circ\text{C}$).

in Figs. 10 and 11. Such modification in the kinetics constant suggests that the mechanism of methane combustion does not occur only in the homogeneous phase, and that sand particles may have a catalytic or inhibitive effect. This is consistent with the previous experiments of Sotudeh-Gharebaagh [21] showing a low catalytic effect of sand particles at temperatures lower than 700°C , and an inhibitive effect at temperatures between 750 and 850°C .

5.2. Effect of operating parameters

The excess air factor and the initial fixed bed height have a very weak effect on the natural gas combustion process. The model matches well this observation [15]. The strong effect of the gas superficial velocity and of the mean particle diameter is correctly predicted by the model, as shown in Fig. 12

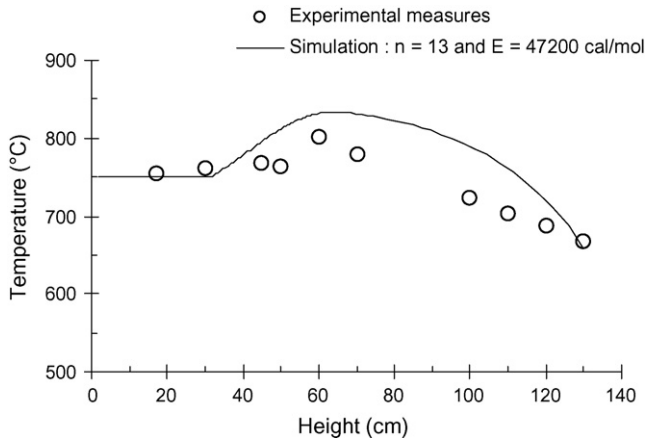


Fig. 10. Temperature profile of gas-particle suspension: comparison between the experimental results and the model predictions ($T_{\text{bed}} = 750^\circ\text{C}$).

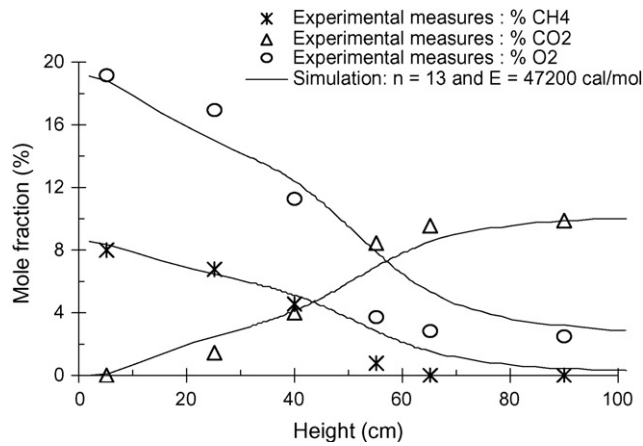


Fig. 11. Mole fraction profiles of the main species present in gas stream: comparison between the experimental results and the model predictions ($T_{\text{bed}} = 750^\circ\text{C}$).

at a dense bed temperature of 700°C . In addition, as shown in Fig. 13, the measured mole fraction profiles are in good agreement with the model predictions for different particles mean sizes.

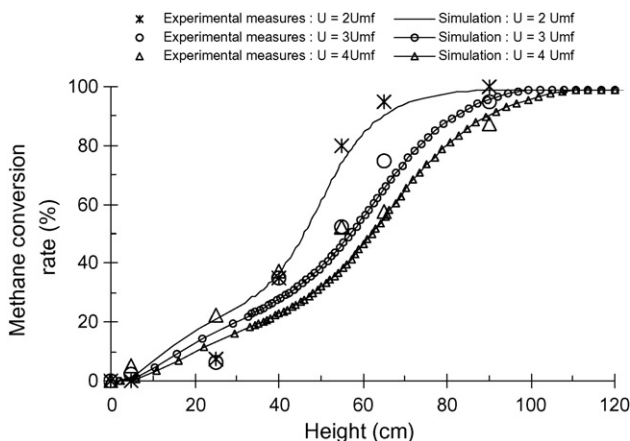


Fig. 12. Comparison between experimental results and model predictions: effect of superficial gas velocity.

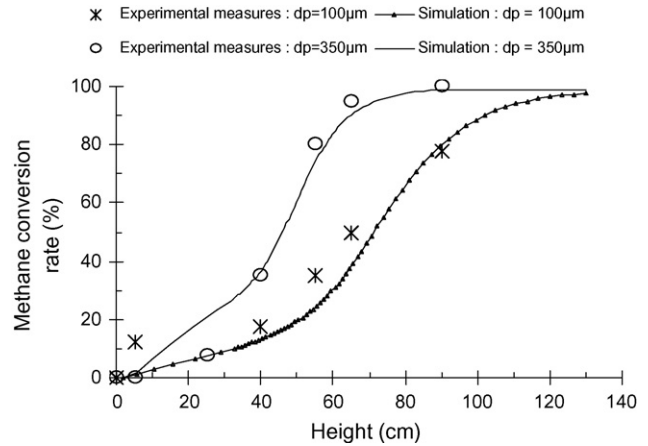


Fig. 13. Comparison between experimental results and model predictions: effect of the mean particle diameter.

6. Conclusion

In the present paper, a theoretical and experimental study of the influence of the freeboard zone on the combustion of natural gas at temperatures lower than the critical temperature have been presented. The experimental study demonstrates the progressive move of the combustion zone towards the dense bed surface and thus into the interior of the dense zone as the bed temperature rises. Increasing the fluidizing velocity or decreasing the mean particle diameter induces the reaction zone displacement towards the reactor outlet. The freeboard modelling combined with the dense bed modelling of Pré et al. [3] predict satisfactorily the reactor behaviour for different operating conditions. At dense bed temperatures lower than the critical temperature, the methane burning is not an exploding phenomenon mainly because of the existence of projected particles. The combustion occurs progressively in the freeboard region and the conversion is total at the reactor outlet. Thus, from a practical point of view, it seems necessary to use coarse particles with mean gas velocities around 12 times the minimum fluidization velocity to ensure achievement of the whole reaction in the reactor and to reach the maximum thermal efficiency of the reactor. The fluidized-bed reactor model gives useful information regarding the thermal efficiency of the operation and permits estimation of the conditions at which the reactor efficiency is maximum.

Appendix A

The gas-particle suspension emissivity $\bar{\varepsilon}_g$ is computed according to the following correlation:

$$\bar{\varepsilon}_g = \varepsilon_p + C_s \varepsilon_g \quad (\text{A1})$$

where ε_g and ε_p are respectively the emissivity of gas and particles. C_s is a factor depending on the gas and solid emissivity, mean diameter and concentration of solid particles.

The particles emissivity is computed, for coarse particles, according to the following correlation:

$$\varepsilon_p = 1 - \exp(-1.5 f_v(L/d_p)) \quad (\text{A2})$$

where L is the characteristic length.

The gas emissivity is calculated using the emissivity of absorbent gas (CO_2 and H_2O) given by the Hottel correlation:

$$\varepsilon_H = C_{\text{CO}_2} \varepsilon_{\text{CO}_2} + C_{\text{H}_2\text{O}} \varepsilon_{\text{H}_2\text{O}} - \Delta\varepsilon \quad (\text{A3})$$

and the use of a blackening factor F_E in order to take into account the presence of species in the gas stream other than CO_2 and H_2O :

$$\varepsilon_g = \frac{F_E - 1 + \varepsilon_H}{F_E} \quad (\text{A4})$$

In these correlations, $\varepsilon_{\text{CO}_2}$ and $\varepsilon_{\text{H}_2\text{O}}$ are the emissivity of carbon dioxide and water vapour, respectively. C_{CO_2} , $C_{\text{H}_2\text{O}}$ and $\Delta\varepsilon$ are factors depending on the partial pressure of gas species, the gas temperature and the characteristic length. The blackening factor for the gas stream is equal to 1.2 according to Bueters et al. [20].

References

- [1] M. Foka, J. Chaouki, C. Guy, D. Klvana, Natural gas combustion in a catalytic turbulent fluidized bed, *Chem. Eng. Sci.* 49 (24A) (1994) 4261–4276.
- [2] S. Dounit, M. Hémati, D. Steinmetz, Natural gas combustion in fluidized bed reactors between 600 and 850 °C: experimental study and modelling of the freeboard, *Powder Technol.* 120 (1/2) (2001) 49–54.
- [3] P. Pré, M. Hémati, B. Marchand, Study of natural gas combustion in fluidized beds: modelling and experimental validation, *Chem. Eng. Sci.* 53 (16) (1998) 2871.
- [4] P. Pré-Goubelle, Contribution à l'étude expérimentale et à la modélisation de la combustion du gaz naturel en réacteur à lit fluidisé, Thèse de Doctorat INP-ENSIGC Toulouse, 1997.
- [5] D.R. Van Der Vaart, Mathematical modelling of methane combustion in a fluidized bed, *Ind. Eng. Chem. Res.* 31 (1992) 999–1007.
- [6] I. Yanata, K.E. Makhorin, A.M. Glukhomanyuk, Investigation and modelling of the combustion of natural gas in a fluidized bed of inert heat carrier, *Int. J. Chem. Eng.* 15 (1) (1975) 68–72.
- [7] A.P. Baskakov, K.E. Makhorin, Combustion of natural gas in fluidized beds, *Inst of Fuel Symposium Series 1: Fluidized Combustion*, C3-1, 1975.
- [8] P.V. Sadilov, A.P. Baskakov, Temperature fluctuations at the surface of a fluidized bed with gas combustion occurring therein, *Int. J. Chem. Eng.* 13 (3) (1973) 449.
- [9] C.Y. Wen, L.H. Chen, Fluidized bed freeboard phenomena: entrainment and elutriation, *AIChE J.* 28 (1) (1982) 117–128.
- [10] A.B. Fournol, M.A. Bergougnou, C.G.J. Baker, Solids entrainment in a large gas fluidized bed, *Can. J. Chem. Eng.* 51 (1973) 401–404.
- [11] F.A. Zenz, N.A. Weil, A theoretical–empirical approach to the mechanism of particle entrainment from fluidized beds, *AIChE J.* 4 (4) (1958) 472–479.
- [12] D. Kunii, O. Levenspiel, Fluidized reactor models: 1. For bubbling beds of fines, intermediate and large particles. 2. For the lean phase: freeboard and fast fluidization, *Ind. Eng. Chem. Res.* 29 (1990) 1226–1234.
- [13] S.E. George, J.R. Grace, Entrainment of particles from aggregative fluidized beds, *AIChE Symp. Ser.* 74 (176) (1978) 67–73.
- [14] F.L. Dryer, I. Glassman, High temperature oxidation of CO and CH_4 , in: *Proceedings of the 14th International Symposium on Combustion*, The Combustion Institute, Pittsburg, 1973, p. 987.
- [15] S. Dounit, Combustion du gaz naturel en réacteur à lit fluidisé: Etude expérimentale et modélisation de la zone dense et de la zone de désengagement, Thèse de Doctorat, INP-ENSIGC, Toulouse, 2001.
- [16] C.K. Westbrook, F.L. Dryer, Simplified reaction mechanisms for the oxidation of hydrocarbon fuels in flames, *Comb. Sci. Technol.* 27 (1981) 31.
- [17] D. Bradley, S.B. Chin, M.S. Draper, G. Hokinson, Aerodynamic and flame structure within a jet-stirred reactor, in: *Proceedings of the 16th Symposium on Combustion*, The Combustion Institute, Pittsburg, 1977, p. 1571.
- [18] K. Kato, C.Y. Wen, Bubble assemblage model for fluidized bed catalytic reactor, *Chem. Eng. Sci.* 24 (1969) 1351–1369.
- [19] D. Kunii, O. Levenspiel, *Fluidization Engineering*, 2nd edition, Butterworth, Heinenman, Boston, 1991.
- [20] K.A. Bueters, J.G. Cogoli, W.W. Habelt, Performance prediction of tangentially fired utility furnaces by computer model, in: *Proceedings of the 15th International Symposium on Combustion*, Tokyo, Japan, 1974.
- [21] Sotudeh-Gharebaagh, Combustion of natural gas in a turbulent fluidized bed reactor, PhD Thesis report, Ecole Polytechnique de Montréal, QC, Canada, 1998.
- [22] W.E. Ranz, W.R. Marshall, *Chem. Eng. Prog.* 48 (1952) 141.